Ilie, R., Girip, I., Ciuncanu, M. and Turley, M., 2016. A Preisach model for hysteretic description of natural maize composites. *Romanian Journal of Technical Sciences - Applied Mechanics, 61*(2), pp.144-160.

A PREISACH MODEL FOR HYSTERETIC DESCRIPTION OF NATURAL MAIZE COMPOSITES

RUXANDRA ILIE[1], IULIAN GIRIP[2], MIHAI CIUNCANU[3], MAX TURLEY[4]

Abstract. The work is focused on the hysteretic behavior of a composite made out of stalk based maize fiber and unsaturated polyester resin polymer as matrix with methyl ethyl ketone peroxide as a catalyst and Cobalt Octoate as a promoter. A Preisach model is used to describe the behavior of such composites subjected to stretching-compression cycles. A procedure for fitting the Bouc-Wen model to imitate experimental data, are presented and discussed together with the Preisach model.

Keywords: composites, natural fiber, hysteretic behaviour, Preisach model, Bouc-Wen model.

1. INTRODUCTION

Several aspects of the hysteretic behavior of composites have already been described by using Bouc-Wen or Duhem models for friction, or Preisach model [1]. The polymers have different mechanical behavior in relation to different kinds of natural fibers. The natural fibers can enhance the properties of polymers as interfacial adhesion, orientation, strength and physical properties. The mechanical properties of polymer composites based on natural fibers depend essentially on the interface adhesion between the fibers and the polymer matrix. This is because natural fibers are rich in cellulose, hemicellulose, pectin and lignin (part of the hydroxyl group) and tend to be strong and hydrophilic (attracts water) while presenting significant hydrophobic polymers (water repelling for reinforced materials with randomly distributed natural fibres of maize (stalk) [2–4].

In this paper, a composite material consisting of maize fibre unidirectionally aligned as shown in Fig.1 and Fig. 2, is considered.

[1] Technical University of Civil Engineering, Bucharest, Romania
[2] Institute of Solid Mechanics of the Romanian Academy
[3] Research Institute for Construction Equipment and Technology ICECON S.A., Bucharest
[4] University of Ulster, UK

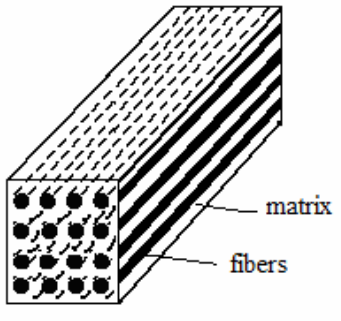

Fig. 1 – A composite rod.

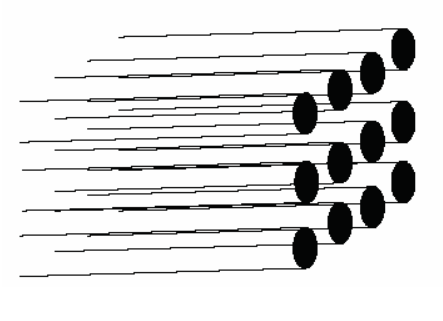

Fig. 2 – Unidirectional maize fibers.

For such composites, the hysteretic behaviour is affected by critical conditions of the non-equilibrium dynamics which occur for separation between the fibre and the matrix [5–9]. Fig. 3 displays a reversal constitutive curve (solid line) with the same value of the strain $\varepsilon = 0.0175$, observed for the copper wires at the unloading-load cycle [10]. Such singularities create non-analyticity in the behaviour at a particular reversal point related to the history of the system. The reversal curves are minor loops, obtained by reversal from ascending or descending branch of the major loops (dotted line).

As results of the discontinuous boundary conditions between fibres and the matrix (including separation between the fibre and the matrix), the hysteretic loops may exhibit the displacement drift, force relaxation and non-closure. Such phenomena can be investigated with the Bouc-Wen model [11]. The unrealistic behavior of the Bouc-Wen model with respect to short input signals was eliminated by inserting a stiffening factor into the hysteretic differential equation. In order to understand the microscopic origin of the reversal effect, the Preisach model can be used [12–17].

In this paper, a Preisach model is used to describe the hysteretic behavior of a composite material consisting of maize fiber unidirectionally aligned. Because we do not have enough experimental data on this composite subjected to stretching-compression cycles [1], we can imitate compatible experimental data starting from an existing set of measurement. For this we consider a system obeying to the law

$$\ddot{x}(t) + r(\dot{x}, x, \theta) + g(t) = 0, \tag{1}$$

where x is the displacement corresponding to the average ultimate strain of composite with unit mass, which depend on the volume fraction, $\dot{x}$ and $\ddot{x}$ are the corresponding velocity and acceleration, respectively, θ is the set of parameters that models the structural behavior, r is a nonlinear restoring force and $g(t)$ is the short unloading-reloading acceleration.

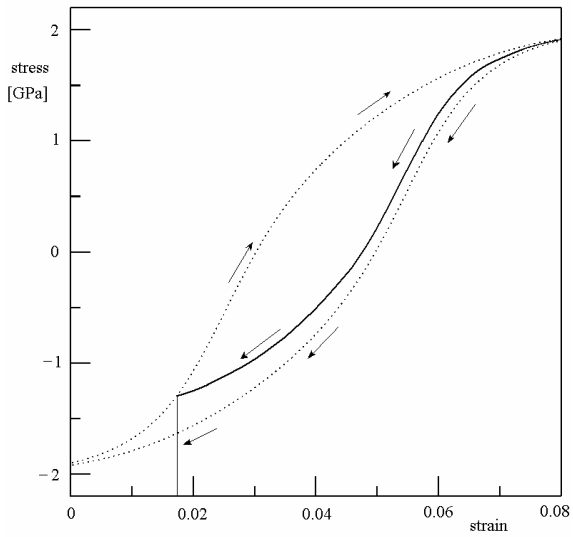

Fig. 3 – Reversal constitutive curve (solid line)
and major hysteretic loop (dotted line).

The restoring force *r* characterizes the hysteretic behavior of the system and we consider that it can be described by the Bouc-Wen model

$$\ddot{r} = c\ddot{x} - k\dot{x} + \beta |\dot{x}| r |r|^{n-1} + (1 - 2H(\dot{x}r)R(x,r))\gamma |\dot{x}| |r|^n, \tag{2}$$

where *c* is the viscous damping coefficient, *k* is the equivalent stiffness coefficient, β and γ are the shape parameters, and *n* governs the smoothness of the force-displacement curve, $R(x,r) \in [0,1]$ is a stiffening factor and $H(\cdot)$ is the Heaviside function defined as

$$H(x) = \begin{cases} 1, & x > 0, \\ 0, & x \le 0. \end{cases}$$

The term $2H(\dot{x}r)R(x,r)$ we can write within the idea that the Heaviside function can help the unloading branches to remain identical to those of the classical model [18, 19].

$$\ddot{r} = c\ddot{x} - k\dot{x} + \beta |\dot{x}| r |r|^{n-1} + \gamma |\dot{x}| |r|^n. \tag{3}$$

Also, the stiffening factor *R* controls the transition between loading (reduced) stiffness and unloading (increased) stiffness, when loading or reloading. For $R = 0$, (2) reduces to (3). For $R = 1$, the loading stiffness becomes equal to that of unloading at the same point.

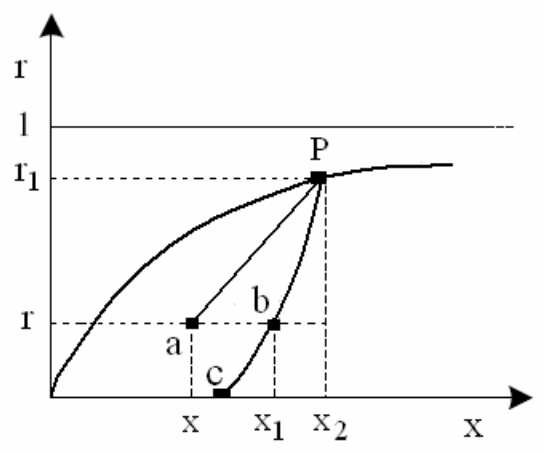

Fig. 4 – The definition of *R*.

We use the Charalampakis and Koumousis definition of *R* [11], and Fig. 4

$$R = H(r_1 - r)H(x_1 - x)\left(\frac{x_2 - x_1}{x_2 - x}\right)^{\kappa}. \tag{4}$$

As shown in Fig. 4, *P* is a reversal point. During reloading, the current state is represented by the point for $0 \le r < r_1$. The point *b* corresponds to the unloading path. As *a* approaches *b* from the left, $R \to 1$. When *a* and *b* coincide, then $R = 1$ and loading follows the unloading path exactly. The unloading path $P - c$ cannot be crossed. When $r > r_1$ or $x > x_1$, the stiffening effect disappears due to the Heaviside function. Parameter controls the intensity of stiffening to the left of the unloading path. The stiffening is closed to the unloading path for increased values of κ, and diminished every where else. It was observed in [11] that $1 \le \kappa \le 2$ is the best for identifying the realistic hysteretic loops. Therefore, the set of parameters θ of the Bouc-Wen model described by (1), (2) and (4), is

$$\theta(t) = [c, k, \beta, \gamma, \kappa], \tag{5}$$

for a given *n* [20].

2. THE PREISACH MODEL

The Preisach model, which describes a hysteretic operator with nonlocal (global) memory, implies mapping of input $u(t)$ on output $f(t)$ in the form [12–14, 21–24].

$$f(t) = \iint_{\alpha \geq \beta} P(\alpha,\beta) G_{\alpha\beta} u(t)\, d\alpha d\beta\,, \tag{6}$$

where $G_{\alpha\beta}$ is an elementary hysteretic operator – a rectangular loop shown in Fig. 5.

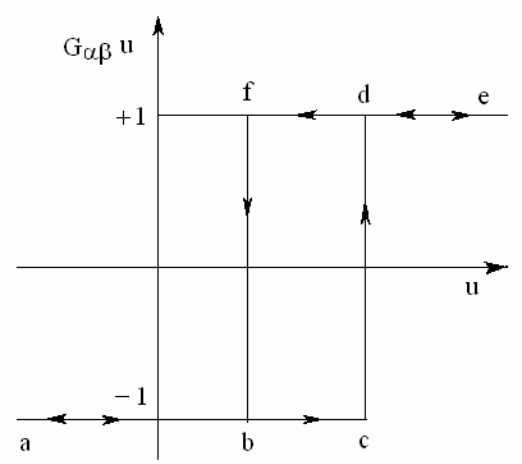

Fig. 5 – Elementary hysteretic operator.

Numbers α and β correspond *up* and *down* switching values of input, respectively $+1$ and -1 are two possible output values. Therefore, in the Preisach model a dynamic system is described as a collection of independent two state ± 1 switching units. As the input $u(t)$ is monotonically increased, the ascending branch *abcde* is followed. When decreased, the descending branch *edfba* is traced. The function $P(\alpha,\beta)$ is named the Preisach function. It is assumed $\alpha \geq \beta$, which is quite natural in the physical point of view. Thus, the integration in (6) is performed over the right triangle in (α,β) plane, with the line $\alpha = \beta$ being the hypotenuse and point $(\alpha_0, \beta_0 = -\alpha_0)$ being the triangular vertex. The value of $\alpha_0 > 0$ is defined by the largest extremum value of the input function $u(t)$.

There is a one-to-one correspondence between $G_{\alpha\beta}$ operators and points(α, β) of the triangle. The triangle (Fig. 6) is called a limiting triangle support for the Preisach function, since the Preisach function $P(\alpha,\beta)$ is assumed to vanish outside the triangle. The interface between two parts of the triangle is a staircase line $L(t)$ whose vertices have (α, β) coordinates that are local input maxima and minima at previous instants of time.

If the input is increasing, the line of $L(t)$ is horizontal; if it is decreasing, it is vertical. At any instant of time the triangle is subdivided into two sets: a positive $A^{+}(t)$ consisting of points (α,β) for which $G_{\alpha\beta}u(t)=1$, and a negative set $A^{-}(t)$ consisting of points (α,β) for which $G_{\alpha\beta}u(t)=-1$, separated by $L(t)$. Thus, equation (6) can be rewritten as

$$f(t)=\iint\limits_{A^{+}(t)} P(\alpha,\beta)\,d\alpha d\beta \;-\; \iint\limits_{A^{-}(t)} P(\alpha,\beta)\,d\alpha d\beta\,. \tag{7}$$

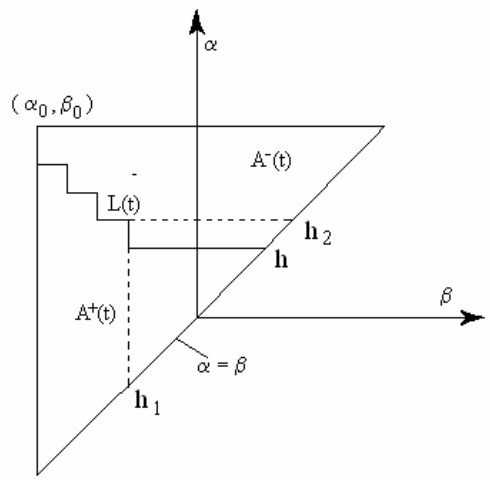

Fig. 6 – Limiting triangle with a staircase interface line $L(t)$.

The model has the following property: each local input maximum wipes out the vertices of $L(t)$ whose α coordinate are below this maximum, and each local minimum wipes out the vertices whose β coordinates are above this minimum. In other words, the Preisach model stores the alternating series of dominant input extrema, while the other extrema are wiped out (Fig. 7). The wiping out of vertices is equivalent to the erasing of the history associated with these vertices. The major hysteretic curve must be defined, at a point h, by the integral (7). Secondary curves are defined by both the primary curve from which it departs, and the point at which it departs from its parent curve, i.e. by two values h_1 and h_2.

All hysteretic loops corresponding to the same extremum values of input are congruent. Such minor loops, obtained by reversal from ascending or descending branch of the major loops, can only be shifted relatively to each other along the output axes. The Preisach function $P(\alpha,\beta)$ can be determined as follows. Starting from the state of negative saturation, let the input be increased to some value α.

The output follows the ascending branch of the major loop, and at input $u = \alpha$ has the value f_α. If the input is subsequently decreased to some value β, the output follows the corresponding reversal (transition) curve.

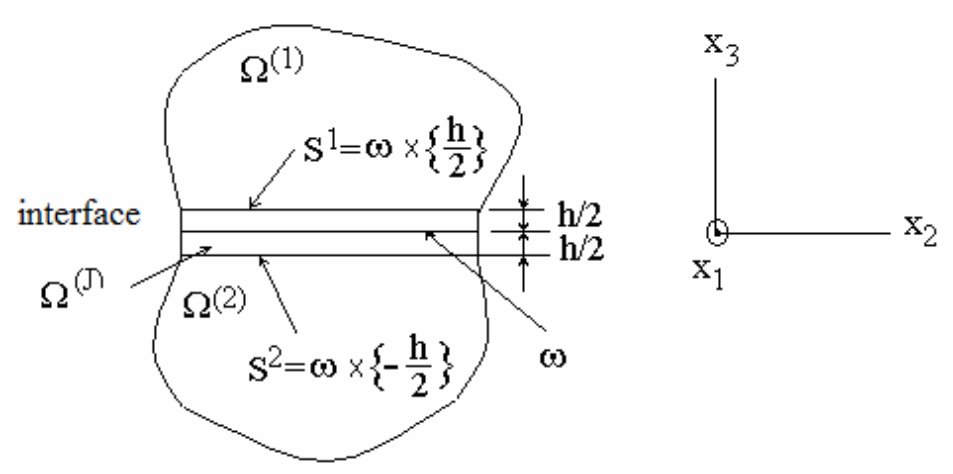

Fig. 7 – The interface model.

Denoting the output value at $u = \beta$ by $f_{\alpha\beta}$, then from the limiting triangle it follows

$$F(\alpha,\beta) = f_{\alpha\beta} - f_\alpha = -2\int_\beta^\alpha \left(\int_\beta^\alpha P(\alpha',\beta')\mathrm{d}\alpha' \right) \mathrm{d}\beta', \tag{8}$$

where by differentiation with respect to β and α, respectively, we have

$$P(-\alpha,-\beta) = P(\alpha,\beta), \quad P(\alpha,\beta) = -\frac{1}{2}\frac{\partial^2 F(\alpha,\beta)}{\partial\alpha\partial\beta}. \tag{9}$$

3. MAIN RESULTS

The composite made out of stalk based maize fiber and unsaturated polyester resin polymer as matrix, has an isotropic structure being free of voids, with reinforcement done by unidirectional fibres, not porous and perfect aligned. Perfect bonding between the fibres and the matrix is assumed [1, 26].

We present a model for the fiber-matrix interface based on the Goland and Reissner's theory [25]. Two bodies called adherents are connected by an adhesive bond that we call the interface. The plane median surface layer is denoted by *w* and its thickness with *h*. We assume that the adhesive material is more flexible than the adherents. The small thickness of the interface and its flexibility lead to neglect the normal stress in the plane interface. Tensions perpendicular to the layer and the shear stresses are constant with respect to thickness.

Let Ω^1 and Ω^2 be regions occupied by the adherents, and Ω^J the interface (Fig. 7). The principle of virtual work gives

$$\iiint\limits_{\Omega^1\cup\Omega^2\cup\Omega^J} \sigma_{ij}\varepsilon_{ij}(u)\,\mathrm{d}V = \iint\limits_{\partial\Omega^1\cup\partial\Omega^2} t_i u_i\,\mathrm{d}S\,, \tag{10}$$

where σ_{ij} are components of the Cauchy stress tensor, ε_{ij} components of the strain tensor, $\varepsilon_{ij}(u) = 1/2(u_{i,j} + u_{j,i})$, u is the displacement vector, and the surface stresses t_i prescribed on $\partial\Omega^1 \cup \partial\Omega^2$. The Hooke law is

$$\sigma_{ij} = \frac{E}{1+\nu}\left(\varepsilon_{ij} + \frac{\nu}{1-2\nu}\varepsilon_{kk}\delta_{ij}\right), \tag{11}$$

where E is the Young's modulus, ν the Poisson ratio, and δ_{ij} the Kronecker symbol. The material properties in the adhesives are denoted by E, ν, and in the adherent $\Omega^1 \cup \Omega^2$ by E_0, ν_0.

The boundary conditions are

$$(\sigma_{ij})_+ = (\sigma_{ij})_- \quad \text{on } \mathrm{S}_1 \cup \mathrm{S}_2\,. \tag{12}$$

As the interface is thin, the assumption of motion variying linearly with thickness, is assumed

$$u_i = u_{0i} + x_3 w_i \quad \text{in } \Omega^J\,, \tag{13}$$

$$u_{0i} = \frac{1}{2}(u_i^1 + u_i^2)\,, \qquad w_i = \frac{1}{h}(u_i^1 - u_i^2)\,, \tag{14}$$

$$u_i^1(x_1, x_2) = u_i(x_1, x_2, h/2)\,, \quad u_i^2(x_1, x_2) = u_i(x_1, x_2, -h/2)\,, \tag{15}$$

The virtual work of the interface W^J

$$\mathrm{W}^J = \iiint\limits_{\Omega^J} \sigma_{ij}\varepsilon_{ij}(u)\mathrm{d}V\,, \tag{16}$$

can be written as

$$W^J = \iint_{\omega}[\int_{\frac{-h}{2}}^{\frac{h}{2}} \sigma_{\alpha\beta} dx_3 a_{\alpha\beta} + \int_{\frac{-h}{2}}^{\frac{h}{2}} \sigma_{\alpha\beta} x_3 dx_3 k_{\alpha\beta} + \int_{\frac{-h}{2}}^{\frac{h}{2}} \sigma_{3\beta} dx_3 (w_\beta + \hat{w}_\beta) + \int_{\frac{-h}{2}}^{\frac{h}{2}} \sigma_{3\beta} x_3 dx_3 s_\beta + \int_{\frac{-h}{2}}^{\frac{h}{2}} \sigma_{33} dx_3 w_3] dx_1 dx_2 , \quad (17)$$

with $a_{\alpha\beta}$, $k_{\alpha\beta}$, $w_\beta + \hat{w}_\beta$, w_3, s_β parameters which describe the deformation of the interface (Fig. 8)

$$a_{\alpha\beta} = \frac{1}{2}(u_{0\alpha,\beta} + u_{0\beta,\alpha}), \quad k_{\alpha\beta} = \frac{1}{2}(w_{\alpha,\beta} + w_{\beta,\alpha}), \quad \hat{w}_\beta = u_{03,\beta}, \quad s_\beta = w_{3,\beta}. \quad (18)$$

The interpretation of these deformations is presented in Fig. 8.

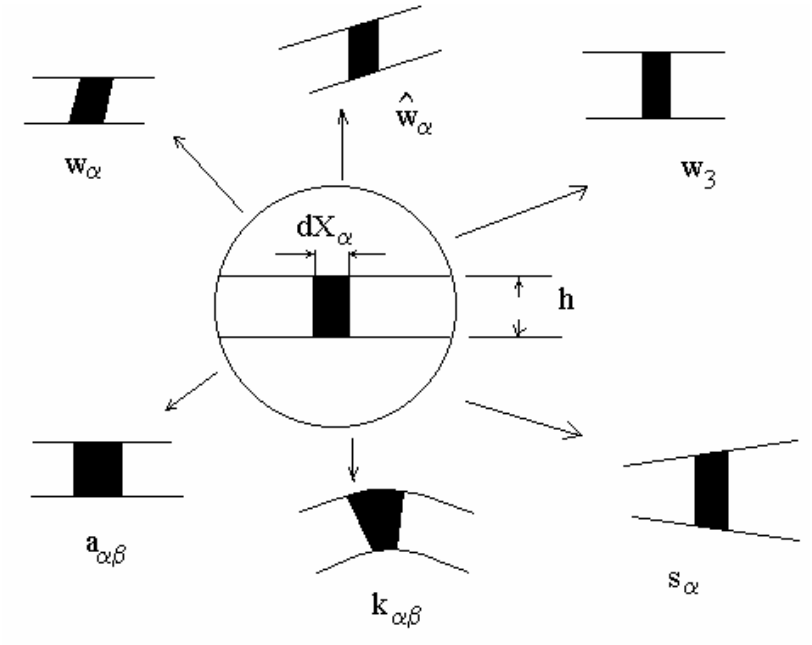

Fig. 8 – Types of the interface deformations.

The interface deformation can be expressed as

$$\varepsilon_{\alpha\beta} = a_{\alpha\beta} + k_{\alpha\beta} x_3, \quad \varepsilon_{3\beta} = (w_\beta + \hat{w}_\beta + s_\beta x_3)/2, \quad \varepsilon_{33} = w_3. \tag{19}$$

The interface is thin (small h), then the stress has the same order of magnitude both in the interface and in constituients, respectively. As the fibers and the matrix are more rezistent than the interface $E_0 >> E$, that is natural to assume $\varepsilon_{\alpha\beta} << \varepsilon_{3j}$. Therefore, $a_{\alpha\beta}$ and $k_{\alpha\beta}$ can be neglected in $(19)_1$. By comparing w_β and $\hat{w}_\beta$ in $(19)_2$, and noticing that w_β prevails in size when h is small, the fourth term of (17) can be neglected. Also, s_β disappears, and a simplified description of the interface deformation results as follows

$$W^J = \iint_\omega \left(\int_{-h/2}^{h/2} \sigma_{3i} \mathrm{d}x_3 w_i \right) \mathrm{d}x_1 \mathrm{d}x_2, \quad \varepsilon_{\alpha\beta} \sim 0, \quad \varepsilon_{3\beta} \sim w_\beta/2, \quad \varepsilon_{33} \sim w_3. \tag{20}$$

Considering the generalised stress $p_i = \int_{-h/2}^{h/2} \sigma_{3i} \mathrm{d}x_3$, we get

$$p_i = C_{ij} w_j, \quad (C_{ij})_{i,j} = \frac{Eh}{1+\nu} \begin{bmatrix} 1/2 & 0 & 0 \\ 0 & 1/2 & 0 \\ 0 & 0 & 1/2 \end{bmatrix}, \quad \sigma_{\alpha\beta} = \delta_{\alpha\beta} \frac{\nu}{h(1-\nu)} p_3, \quad \sigma_{3i} = \frac{1}{h} p_i. \tag{21}$$

The potential imperfect bonding between fibre and matrix referring to fibre-matrix separation, are undesirable because they lead to weakening the integrity of the composite. materials with poor fibre content considered. The fibre is an isotropic material with Young's modulus $E_f = 8.58$ GPa. The matrix is a polymeric resin with Young's modulus $E_m = 1.3$ GPa, and Poisson ratio $\nu_m = 0.3$. The volume fibre content is varying from 20 to 25%. The level of stress in the fiber is lower and in the matrix is higher than in the composite with low fibre content. The average value of the composite are computed using the Halpin-Tsai, Nielson and Cox models. The Halpin-Tsai equation is often used for short-fiber reinforced composite [25, 26]

$$\frac{P}{P_m} = \frac{1+\zeta\eta V_f}{1-\eta V_f}, \tag{22}$$

where P represents any one of the composite moduli such as the longitudinal moduli (E_f, E_m) for which $\zeta = 2(l/d)$, with l/d the fiber aspect ratio, the transverse moduli for which $\zeta = 2$, and longitudinal shear moduli (G_f, G_m) for which $\zeta = 1$, P_f and P_m are the corresponding moduli of the fiber and matrix, respectively, ζ is a parameter that depends on the particular property being considered, and $\eta = \frac{(P_f/P_m)-1}{(P_f/P_m)+1}$.

The Nielson model changes the Halpin-Tsai equation as [27]

$$E_c = E_m \frac{1+2s\eta V_f}{1-\psi\eta V_f}, \tag{23}$$

$$T_c = T_m \frac{1+2s\eta^* V_f}{1-\psi\eta^* V_f}, \tag{24}$$

where

$$\psi = 1 + V_f \frac{1-\phi_{\max}}{\phi_{\max}^2}, \quad \eta = \frac{E_f - E_m}{E_f + 2sE_m}, \quad \eta^* = \frac{R_f - R_m}{R_f + 2sR_m}. \tag{25}$$

Here, E_c, E_f and E_m are the moduli of the composite, fiber and matrix, respectively, T_c, T_f and T_m are the strength of the composite, fiber and matrix, respectively. The parameter $\Phi_{\max}$ is the maximum packing fraction of the reinforcement. The Cox model [28] is a micromechanical model for short fibers oriented:

$$E_{11} = \eta_l V_f E_f + (1-V_f)E_m, \tag{26}$$

where

$$\eta_l = 1 - \frac{\tanh(\beta l/2)}{\beta l/2}, \quad \beta = \sqrt{\frac{H}{\pi r_f^2 E_f}}, \quad H = \frac{2\pi G_m}{\ln(R/r_f)}, \quad R = r_f\sqrt{\frac{K_R}{V_f}}. \tag{27}$$

where E_f, E_m are the moduli of the fiber and matrix, respectively, G_m is the shear modulus of the matrix, and η_l is a length dependent efficiency factor, K_R is a constant and is usually chosen to be one.

To imitate the experimental data, the Bouc-Wen parameters $\theta = [c, k, \beta, \gamma, \kappa]$ are chosen to be

$$c = 0.07 \text{ kNs/m}, \quad k = 25 \text{ kN/m}, \quad \beta = 2, \quad \gamma = 1, \quad \kappa = 1.5.$$

The parameter n is kept constant ($n = 2$).

The available experimental measurements refer to force-displacement data for of beams (Figs. 9, 10, 11) reinforced with natural fibres such as basalt, hemp and maize, for different values of fibre volumetric fraction [29].

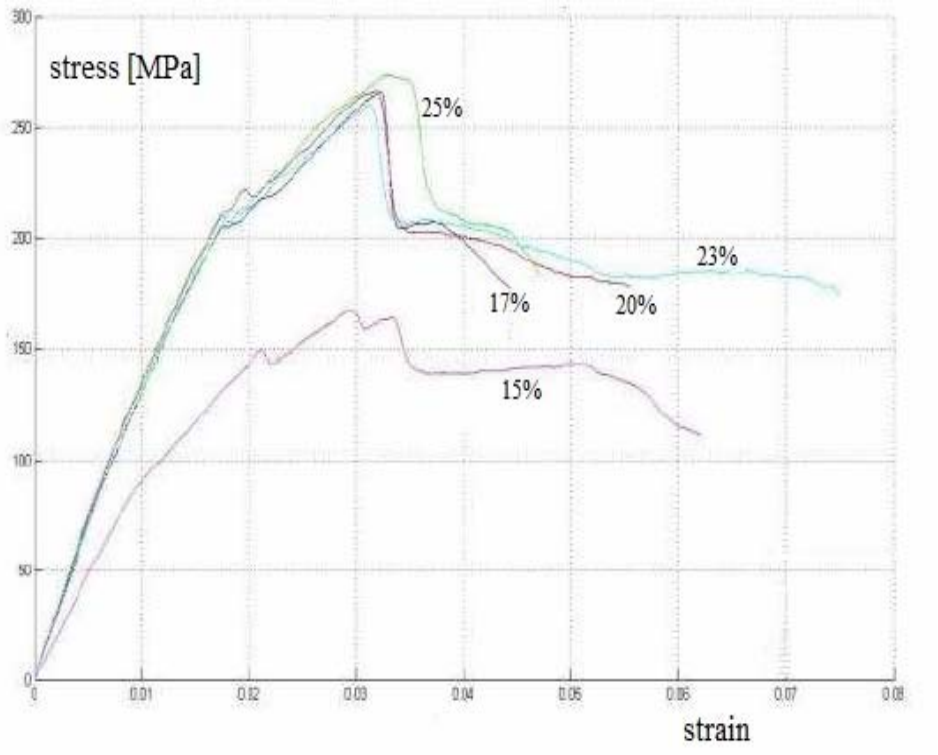

Fig. 9 – Experimental force-displacement
of a beam reinforced with basalt fibers.

Figure 12a shows the experimentally measured displacement for the maize composite. The prediction errors are shown in Fig. 12b. Clearly, the Bouc-Wen model is accurate.

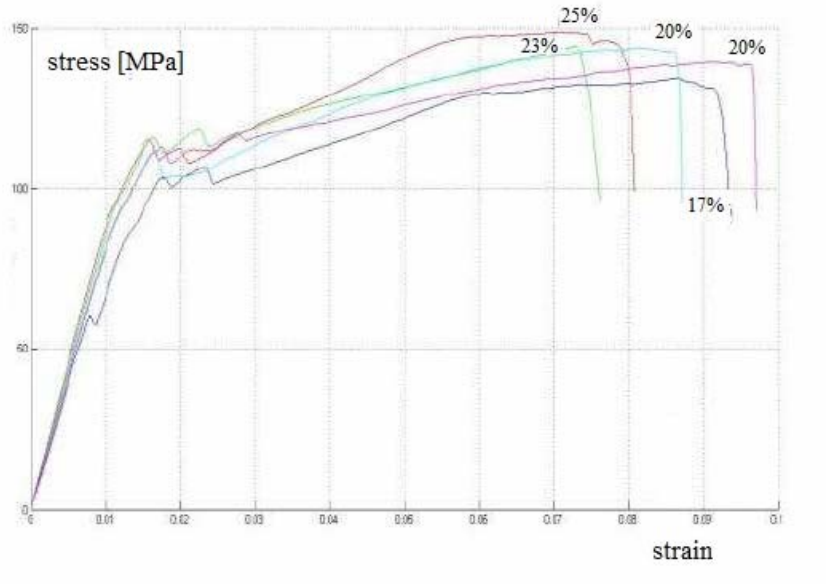

Fig. 10 – Experimental force-displacement
of a beam reinforced with hemp fibers.

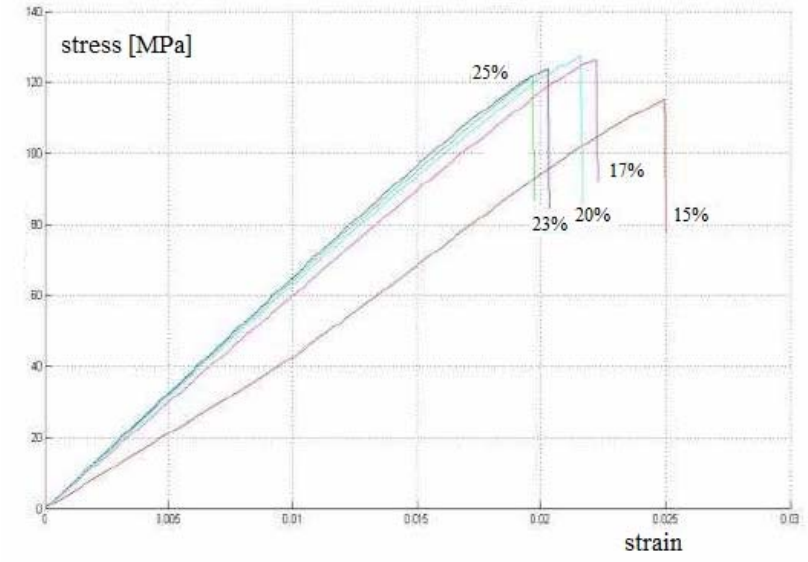

Fig. 11 – Experimental force-displacement
of a beam reinforced with maize fibers.

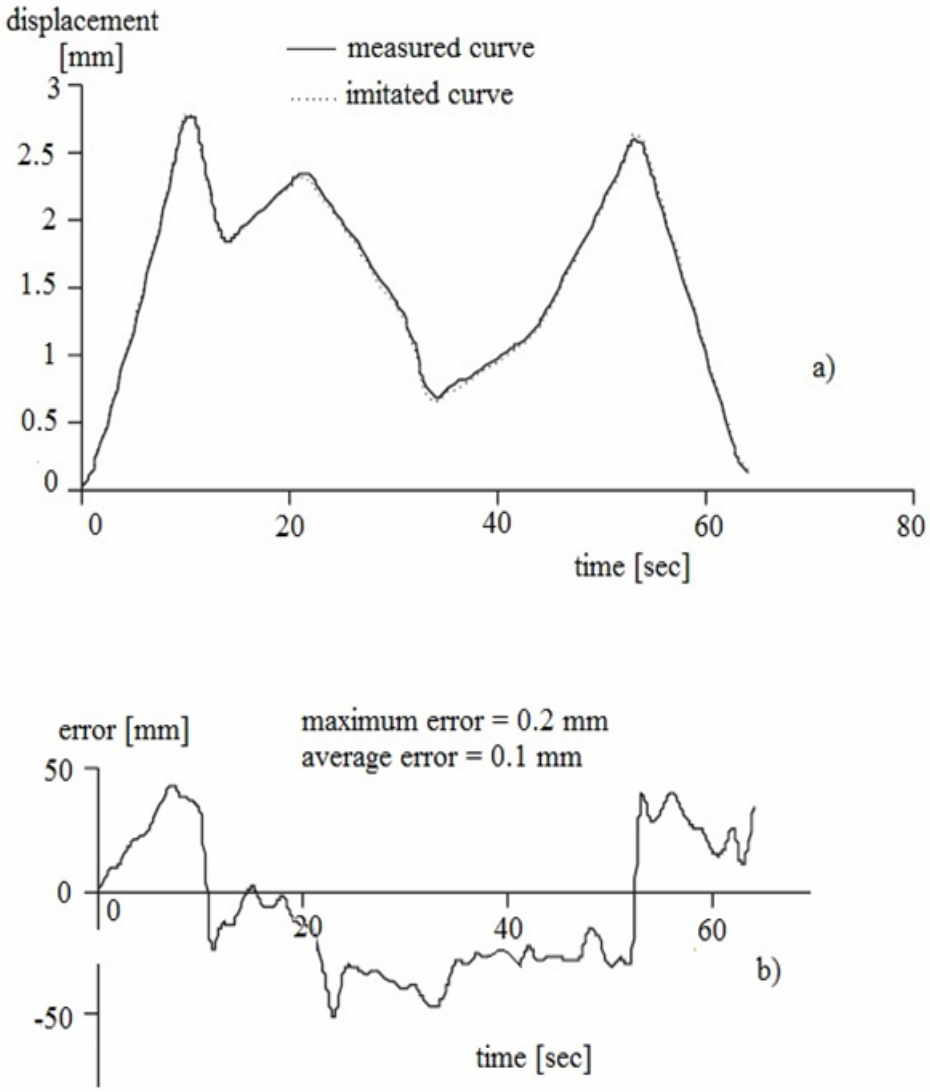

Fig. 12 – a) Measured and imitated values
of displacement variation in time; b) prediction errors.

The central result of the Preisach modeling is presented in Fig. 13 for maize composites, after: a) 4; b) 9; c) 15; d) 20; e) 30, and f) 45 cycles.

We observe, that the strain energy increases with the increase of deformation according to traditional composites, and the composite can sustain large enough deformations without failure.

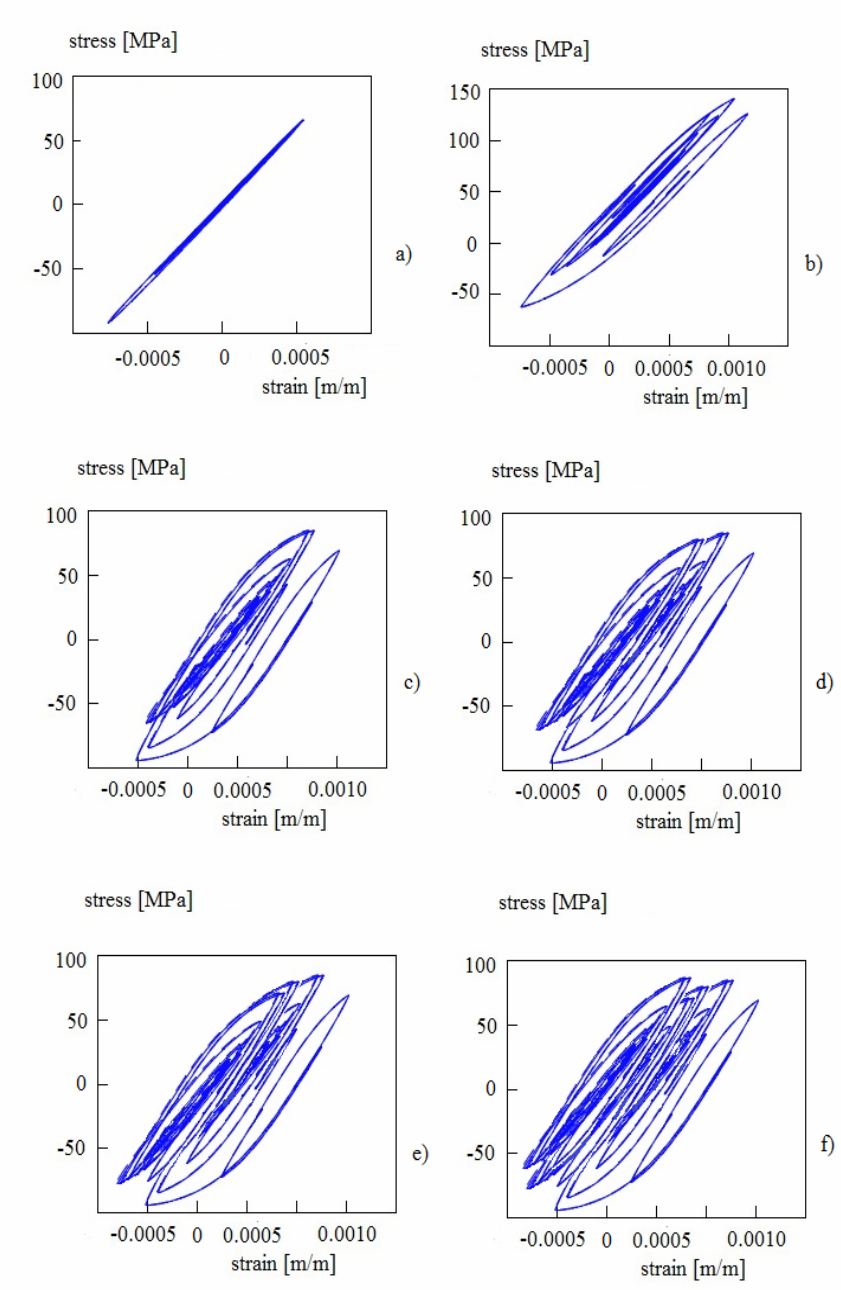

Fig. 13 – Force-displacement loops for a beam reinforced with maize fibers: a) 4; b) 9; c) 15; d) 20; e) 30, and f) 45 cycles.

4. CONCLUSIONS

The presented Preisach model captures hysteresis in a composite made out of stalk based maize fiber and unsaturated polyester resin polymer as matrix with methyl ethyl ketone peroxide as a catalyst and Cobalt Octoate as a promoter.

The model is implemented using a numerical technique based on a Bouc-Wen model to imitate missed experimental data. The main advantage of the model is associated with its simple working, allowing describing of the hysteretic behavior based on measurement results. The Preisach model remains a good model for hysteresis in composites where the load fluctuation is relatively small and the range of the excitation is limited.

Acknowledgements. The authors gratefully acknowledge the financial support of the National Authority for Scientific Research ANCS/UEFISCDI through the project PN-II-ID-PCE-2012-4-0023, Contract no. 3/2013.

Received on June 2, 2016

REFERENCES

1. SARAVANA BAVAN, D., MOHAN KUMAR. G.C., *Finite Element Analysis of a natural fiber (maize) composite beam*, Hindawi Publishing Corporation, Journal of Engn., Article ID 450381, 2013.
2. VAJARI, D.A., *Micromechanical failure in fiber-reinforced composite*s, PhD Thesis, Technical University of Denmark, 2014.
3. ILIE, R., CHIROIU, V., *On the natural fiber (maize) composite material*, PAMM - Proceedings in Applied Mathematics and Mechanics, **15**, *1*, pp. 303–304, 2015.
4. ILIE, R., *On the composites consisting of randomly distributed fibers*, PAMM - Proceedings in Applied Mathematics and Mechanics, **16**, *1*, pp. 351–352, 2016.
5. KATZGRABER, H.G., PÁZMÁNDI, F., PIKE, C.R., LIU, K., SCALETTAR, R.T., VEROSUB, K.L., ZIMÁNYI, G.T., *Reversal-field memory in the hysteresis of spin glasses*, Physical Review Letters, **89**, *25*, p. 257202, 4 pages, 2002.
6. OH, J.H., PADTHE, A.K., BERNSTEIN, D.S., RIZOS, D.D., FASSOIS, S.D., *Duhem models for hysteresis in sliding and pre sliding friction*, Proceedings of the 44th IEEE Conference on Decision and Control, and the European Control Conference 2005, Seville, Spain, Dec. 12–15, 2005.
7. KOROBOV, A.I., EKONOMOV, A.N., *Singularities of nonlinear acoustic properties of copper wires in the field of plastic strains at a unloading-load*, XI Session of the Russian Acoustical Society, Moscow, Nov. 19–23, 2001, pp. 109–112.
8. CUI, T., LIAO, W., YU, D., *Topological approach for analyzing and modeling the aerodynamic hysteresis of an airfoil*, CMES: Computer Modeling in Engineering & Science, **45**, *3*, pp. 273–293, 2009.
9. PREDA, V., IONESCU, M.F., CHIROIU, V., *A Preisach model for the analysis of the hysteretic phenomena*, Romanian Journal of Technical Sciences – Applied Mechanics, **55**, *3*, pp. 243–254, 2010.

10. DELSANTO, P.P., MUNTEANU, L., CHIROIU, V., Private Communication, Politecnico di Torino, 2009.
11. CHARALAMPAKIS, A.E., KOUMOUSIS, V.K., *A Bouc-Wen model compatible with plasticity postulates*, Journal of Sound and Vibration, **322**, *4*, pp. 954–968, 2009.
12. PREISACH, F., *Uber die magnetische Nachwirkung*, Z. Physics, **94**, pp. 277–302, 1935.
13. MAYERGOYZ I.D., *Mathematical models of hysteresis*, Springer-Verlag, New-York, 1991.
14. KRASNOSELSKY, M., POKROVSKY, A., *Systems with hysteresis* (in Russian), Nauka, Moskva, 1983.
15. GUYER, R., MCCALL, K., BOITNOTT, G., HILBERT, L., PLONA, T., *Quantitative implementation of Preisach-Mayergoys space to find static and dynamic elastic moduli in rock*, J. of Geophysical Research, **102**, B3, p. 5281, 1997.
16. BADEA, T., CHIROIU, V., MUNTEANU, L., DONESCU, St., *A Preisach model of hysteretic behaviour of nonlinear mesoscopic elastic materials*, Rev. Roum. Sci. Techn. – Méc. Appl., **47**, *1–6*, pp. 83–96, 2002.
17. CHIROIU, V., MUNTEANU, L., *A model for identification of hysteretic behaviour of materials*, Proceedings of the 8th WSEAS Int. Conf. on Non-Linear Analysis, Non-Linear Systems and Chaos, 2009, pp. 310–315.
18. GLIOZZI, A, MUNTEANU, L., SIRETEANU, T., CHIROIU, V., *An identification problem from input-output data*, Rev. Roum. Sci. Techn. – Méc. Appl., **55**, *3*, pp. 219–232, 2010.
19. CHANG, C.C., SHI, Y., *Identification of time-varying hysteretic structures using wavelet multiresolution analysis*, International Journal of Non-Linear Mechanics, **45**, *1*, pp. 21–34, 2010.
20. SIRETEANU, T., GIUCLEA, M., MITU, A.M., *Identification of an extended Bouc-Wen Model with application to seismic protection through hysteretic devices*, Computational Mechanics, **45**, *5*, pp. 431–441, 2009.
21. BADEA, T., NICOLESCU, C.M., *A Preisach model of hysteretic behavior of nonlinear mesoscopic elastic materials* (Ch.1), in: *Topics in Applied Mechanics* – Vol.1 (Eds. V. Chiroiu and T.Sireteanu), Romanian Academy Publishing House, Bucharest, 2003, pp. 1–26.
22. DONESCU, St., MUNTEANU, L., GIRIP, I., *Hysteresis in the shape memory alloys*, Rev. Roum. Sci. Techn. – Méc. Appl., **56**, *3*, pp. 296–308, 2011.
23. MUNTEANU, L., DELSANTO, P.P., MITU, A.M., CHIROIU, V., *On the modeling of Euler-Bernoulli beams with auxetic patchs*, Rev. Roum. Sci. Techn. – Méc. Appl., **53**, *2*, pp. 211–220, 2008.
24. DONESCU, St., CHIROIU, V., MUNTEANU, L., *On the evaluation of the Young's modulus for a laminated periodic composite structure based on auxetic materials*, Rev. Roum. Sci. Techn. – Méc. Appl., **53**, *3*, pp. 309–320, 2008.
25. GOLAND, M., REISSNER, E., *The stresses in cemented joints*, Journal of Applied Mechanics, **66**, A17-A27, 1944.
26. ILIE, R., *On the composites consisting from random distributed fibres. Theory and experiment*. PhD Thesis, Institute of Solid Mechanics of the Romanian Academy, 2015.
27. ASHTON, J.E., HALPIN, J.C., PETIT, P.H., *Primer on composite materials*: *Analysis*, Technomic Stamford, Connecticut, US, 1969.
28. HALPIN, J.C., *Stiffness and expansion estimates for oriented short fiber composites*, Journal of Composite Materials, **3**, *4*, pp. 732–734, 1969.
29. NIELSON, L.E., *Mechanical properties of polymer and composites*, Vol. 2, New York, Marcel Dekker, 1974.
30. COX, H.L., *The elasticity and strength of paper and other fibrous materials*, British Journal of Applied Physics, **3**, *3*, pp. 72–79, 1952.